

Cavity enhanced absorption spectroscopy using a broadband prism cavity and a supercontinuum source

Paul S. Johnston and Kevin K. Lehmann*

¹Department of Chemistry University of Virginia McCormick Rd Charlottesville, VA 22904, USA, USA

*Corresponding author: lehmann@virginia.edu

Abstract: We report the design and construction of a cavity enhanced absorption spectrometer using broadband Brewster's angle prism retroreflectors and a spatially coherent 500 nm to >1.75 μm supercontinuum excitation source. Using prisms made from fused silica an effective cavity reflectivity of >99.99% at 1.064 μm was achieved. A proof of principle experiment was performed by recording the cavity enhanced absorption spectrum of the weak b-X ($1\leftarrow 0$) transition of molecular oxygen at 14529 cm^{-1} and the fifth overtone of the acetylene C-H stretch at 18430 cm^{-1} . CCD frames were integrated for 150 sec and 30 sec, with 3 frames (each 100 cm^{-1} wide) and 1 frame (266 cm^{-1} wide) required to observe the O_2 and C_2H_2 spectra, respectively. A rms noise equivalent absorption (α_{min}) of $7.21 \times 10^{-8} \text{ cm}^{-1} \text{ Hz}^{-1/2}$ and $1.28 \times 10^{-7} \text{ cm}^{-1} \text{ Hz}^{-1/2}$ with full width half maximum line widths of 0.18 cm^{-1} and 0.44 cm^{-1} were achieved for the molecular oxygen band and the acetylene overtone, respectively.

©2008 Optical Society of America

OCIS codes: (300.0300) Spectroscopy; (010.1030) Absorption; (120.0120) Instrumentation, measurement, and metrology; (140.4780) Optical resonators; (190.0190) Nonlinear optics.

References and links

1. A. O'Keefe and D. A. G. Deacon, "Cavity ring-down optical spectrometer for absorption-measurements using pulsed laser sources," *Rev. Sci. Instrum.* **59**

13. W. J. Wadsworth, N. Joly, J. C. Knight, T. A. Birks, F. Biancalana, and P. S. J. Russell, "Supercontinuum and four-wave mixing with Q-switched pulses in endlessly single-mode photonic crystal fibres," *Opt. Express* **12**, 299-309 (2004).
14. J. M. Langridge, T. Laurila, R. S. Watt, R. L. Jones, C. F. Kaminski, and J. Hult, "Cavity enhanced absorption spectroscopy of multiple trace gas species using a supercontinuum radiation source," *Opt. Express* **16**, 10178-10188 (2008).
15. S. E. Fiedler, A. Hese, and A. A. Ruth, "Incoherent broad-band cavity-enhanced absorption spectroscopy," *Chem. Phys. Lett.* **371**, 284-294 (2003).
16. S. M. Ball, I. M. Povey, E. G. Norton, and R. L. Jones, "Broadband cavity ringdown spectroscopy of the NO₃ radical," *Chem. Phys. Lett.* **342**, 113-120 (2001).
17. K. K. Lehmann, Department of Chemistry, University of Virginia, Charlottesville, VA 22904, P. S. Johnston and P. Rabinowitz are preparing a manuscript to be called "Design and analysis of Brewster's angle prism retroreflectors for cavity enhanced spectroscopy".
18. M. Bass, ed., *Handbook of Optics Volume II - Devices, Measurements, and Properties*, 2nd ed. (McGraw-Hill), Vol. 2.
19. C. Xiong and W. J. Wadsworth, "Polarized supercontinuum in birefringent photonic crystal fibre pumped at 1064 nm and application to tuneable visible/UV generation," *Opt. Express* **16**, 2438-2445 (2008).
20. W. Becker, *Advanced time-correlated single photon counting techniques* (Springer, New York, 2005).
21. S. Schroder, M. Kamprath, A. Duparre, A. Tunnermann, B. Kuhn, and U. Klett, "Bulk scattering properties of synthetic fused silica at 193 nm," *Opt. Express* **14**, 10537-10549 (2006).
22. G. J. Scherer, K. K. Lehmann, and W. Klemperer, "The high-resolution visible overtone spectrum of acetylene," *J. Chem. Phys.* **78**, 2817-2832 (1983).
23. L. S. Rothman, *et al.*, "The HITRAN 2004 molecular spectroscopic database," *J. Quant. Spectrosc. Radiat. Transfer* **96**, 139-204 (2005).
24. J. S. Wong, "Pressure Broadening of single vibrational-rotational transitions of acetylene at $\nu=5$," *J. Mol. Spectrosc.* **82**, 449-451 (1980).
25. H. Chen and W. B. Yan, "Prism-based cavity ringdown spectroscopy: broadband and ultrahigh reflectivity," in *62nd International Symposium on Molecular Spectroscopy* (The Ohio State University Columbus, OH, 2007), <http://hdl.handle.net/1811/31394>.
26. T. Schreiber, J. Limpert, H. Zellmer, A. Tunnermann, and K. P. Hansen, "High average power supercontinuum generation in photonic crystal fibers," *Opt. Commun.* **228**, 71-78 (2003).
27. E. Hamers, D. Schram, and R. Engeln, "Fourier transform phase shift cavity ring down spectroscopy," *Chem. Phys. Lett.* **365**, 237-243 (2002).
28. A. A. Ruth, J. Orphal, and S. E. Fiedler, "Fourier-transform cavity-enhanced absorption spectroscopy using an incoherent broadband light source," *Appl. Opt.* **46**, 3611-3616 (2007).

1. Introduction

The use of high finesse optical cavities to enhance the sensitivity of absorption spectroscopy has greatly expanded since the introduction of Cavity Ring-Down Spectroscopy (CRDS) by Deacon and O'Keefe [1]. CRDS and related methods, including Cavity Enhanced Absorption Spectroscopy (CEAS) [2, 3] and NICE-OHMS [4], exploit the sensitivity of the decay rate and transmission of low loss optical cavities to a small additional loss, due to absorption or scattering, introduced by a sample inserted inside the optical resonator. In almost all of this work, dielectric mirrors have been used to create the cavities because of the ability to obtain "super mirrors" with losses of less than 100 parts per million [5]. With the proper choice of materials for the layers, dielectric mirrors can be constructed over a wide range of wavelengths and can achieve low loss in the spectral region between the mid-IR through the near-UV. The high reflectivity of such mirrors is achieved by constructive interference of the Fresnel reflection of many interfaces produced by multilayer coatings of alternate high and low index materials. Consequently, the wavelength coverage of the highest reflectivity mirrors is limited to only a few percent of a central design wavelength. Larger bandwidths have been demonstrated using chirped mirrors but at the expense of reduced peak reflectivity [6-8].

Here we report on the design and construction of a new type of cavity enhanced spectrometer that uses broadband Brewster's angle retroreflector prisms in place of the high reflectivity mirrors, as first reported in a conference paper [9]. The prisms, based on Brewster's angle and total internal reflection, form a high finesse optical cavity [10, 11] with a theoretical bandwidth limited only by the low internal transmission loss region of the material used to construct the prisms. Pipino *et al.* previously used internal reflection in monolithic

prism cavities for evanescent wave absorption CRDS [12]. We demonstrate the low optical loss bandwidth of our prism resonator by using the visible portion (500-795 nm) of a “white light” supercontinuum excitation source [13]. Except for a publication that appeared just as we were about to submit the present paper for publication [14], this work demonstrates the use of such a source to perform cavity enhanced spectroscopy. In that work, high reflectivity mirrors were used, reducing the bandwidth of the spectrometer to 100 nm or <7% of the source bandwidth.

2. Experimental details

Figure 1 shows the general configuration of the spectrometer. The spectrometer consists of three major components: the prism based optical resonator, a supercontinuum source, and a spectrograph based detection system, each of which will be described in more detail. For this initial demonstration, we use the cavity enhanced absorption spectroscopy [2, 3, 15] method. This method, unlike CRDS, does not require simultaneous detection of cavity decay transients over many wavelengths. Eq. (1) shows how the absolute absorption strength of a sample inside the cavity, $\alpha(\nu)$, vs. light frequency, ν , can be calculated. Here $I(\nu)$ is the measured spectrum of light transmitted by the cavity with the sample; $I^o(\nu)$ is the measured spectrum of light transmitted by the empty cavity; $\tau(\nu)$ is the empty cavity photon lifetime (ring-down time); c is the speed of light; $n(\nu)$ is the index of refraction of the prisms; L_p is the single pass path length inside a prism; L_g is the path length in the gas.

$$\alpha(\nu) = (c\tau(\nu))^{-1} \left(1 + n(\nu) \frac{L_p}{L_g} \right) \left(\frac{I^o(\nu)}{I(\nu)} - 1 \right) \quad (1)$$

The factor $(1 + n L_p/L_g)$ corrects for the fraction of time the photons spend in the sample. This approach could be combined with a special gated CCD camera described by Ball and Jones [16] capable of measuring and signal averaging on silicon 512 parallel ringdown events. Thus, the photoelectrons from many pulses can be added until the point that the shot noise dominates over the read out noise of the CCD, permitting multiplexed CRDS measurements across the entire spectrum sampled by the CCD.

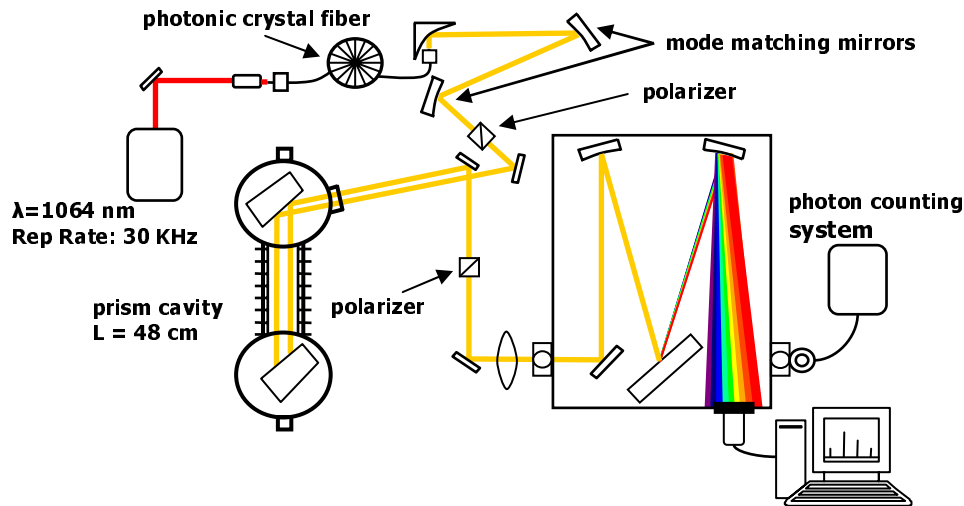


Fig. 1. Schematic of the cavity enhanced absorption spectrometer showing the major components of the spectrometer: the supercontinuum source, the broadband Brewster's angle retroreflector prism cavity, and the dispersive grating spectrograph.

2.1 Prism cavity

Discussed here is only a general analysis of the prism cavity. A more detailed analysis will be presented in a future publication, including ABCD beam propagation calculations and an alignment and manufacturing error analysis [17]. A stable optical cavity is formed by two Brewster's angle retroreflectors facing each other such that corresponding faces are nearly parallel. A top view illustration of the prism cavity is shown in Fig. 2. The prisms were fabricated from Suprasil 3001, a low OH⁻ fused silica (~1 ppm [OH⁻]), by the Australian Centre for Precision Optics. Fused silica was selected because of its availability in high purity and highly homogeneous forms and for the material's low dispersion profile across the visible and near-IR spectral region. Each of the intracavity optical surfaces, of which there are three per prism, have been super polished (<1 Å rms roughness, 0-0 scratch and dig) to minimize surface scattering losses. Let $\theta_B = \tan^{-1}(n)$ where $n = 1.45$ is the index of refraction of fused silica. The prism dimensions (in mm) are AB = 16.0, BC = 20.3, CD = 13.5, AD = 27.5 and a height of 14.0. The angles are $\angle ABC = 90^\circ$, $\angle BAD = 135^\circ - \theta_B = 79.6^\circ$ (selected so a ray entering surface AB at Brewster's angle will strike surface AD at 45°), $\angle BCD = 3\theta_B - 45^\circ = 121.2^\circ$ (selected so the input beam will pass through surface CD also at Brewster's angle). The second prism is identical except that surface EF has a $R_c = 6$ m convex radius of curvature. The optic axis will strike this surface (R_2) where the local normal to the surface is exactly parallel to line GF. Due to the Brewster angle surfaces and because the beam strikes the curved surface (EF) at 45° , the focusing is highly astigmatic, with the curved prism having effective focal lengths of $\frac{R_c}{\sqrt{8n^3}}$ and $\frac{R_c}{\sqrt{2n}}$ for in-plane (t) and out-of-plane (s) rays. The cavity is stable for single pass optical lengths less than $\frac{R_c}{\sqrt{2n^3}} = 1.39$ m.

Tracing the optical path of one round trip of the cavity starting at the point R_0 in Fig. 2, light polarized in the plane of incidence, p -polarized, is incident to the surface AD of the prism at nearly Brewster's angle, coupling by reflection a small fraction of the input beam into the cavity with the majority of the light being transmitted through the prism into a beam dump. By rotating the input prism we are able to control the fractional reflectivity of surface AD and therefore able to adjust the cavity coupling losses. The fractional reflected intensity as a function of Brewster's angle detuning is given by:

$$R(\lambda) = \frac{(n(\lambda)^4 - 1)^2}{4n(\lambda)^6} \delta\theta(\lambda)^2 \quad (2)$$

where $R(\lambda)$ is the fractional reflected intensity, $n(\lambda)$ is the prism material index of refraction [18] and $\delta\theta(\lambda)$ is the detuning angle from Brewster's angle. For example, for a typical detuning angle of 1° from Brewster's angle, a fractional reflected intensity of 100 parts per million is predicted.

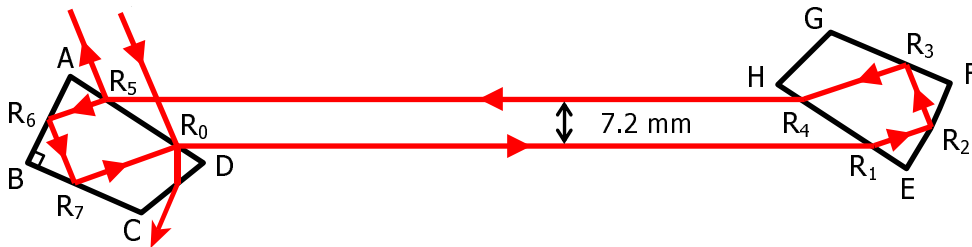


Fig. 2. A schematic of the Brewster angle retroreflector based ring cavity showing the optical beam path. Light is coupled into the cavity at R_0 and decoupled at R_5 . All surfaces are flat except EF which has a 6 m convex curve. Labels are referred to in the text along with prism dimensions and angles. The effective reflectivity of the cavity is controlled by tuning the input prism around Brewster's angle.

Upon reflection, the beam propagates the length of the cavity, $L_g = 48$ cm, and strikes the surface label EH (point R_1) at Brewster's angle, transmitting the beam into the prism and ideally suffering no reflection loss for a given wavelength. Entering the prism, the beam undergoes two total internal reflections at points R_2 , R_3 . These prisms are design such that the beam is incident to the dielectric/air interface at an angle greater than the critical angle. For example, the calculated critical angle for fused silica ranges from 43.14° to 44.24° for the wavelength range of 500 nm to $2.30 \mu\text{m}$, smaller than the designed 45° incident angle. The internal reflection surface EF has been polished with a 6 m radius of curvature, providing a focusing element to form a stable optical cavity. The beam is again transmitted out of the prisms by Brewster's angle at R_4 on surface EH. The total intraprism path length per prism is $L_p = 38.3$ mm. Exiting the prism, the beam again propagates the length of the cavity. The exiting beam is parallel to the beam at R_1 and displaced by 7.2 mm. The beam then hits the surface AD at the same angle as the cavity input beam, decoupling a small fraction of light from the cavity at R_5 that is sent to the monochromator for detection, transmitting the majority of the light into the prism where it sequentially undergoes another 2 internal reflections at points R_6 and R_7 on the flat surfaces AB and BC. The surfaces AB and BC form a 90° angle in the prism such that the beam exits the prism at point R_0 and is parallel to the beam at point R_5 . In the described system the cavity round trip time at $1.064 \mu\text{m}$ is 3.6 ns, including the propagation time inside the prisms, yielding a free spectral range of approximately 290 MHz.

The prisms are mounted inside a 660 cm^3 vacuum chamber pumped by a 160 l/min mechanical pump. Each prism is contained in separate compartments with each compartment secured to a commercial prism stage (Newport PO80). The two prism compartments are joined using two bellows. Figure 3 shows a schematic of the vacuum chamber. A 0.4 cm thick quartz plate was used to separate the prism from the vacuum chamber mounting surface, minimizing any stress induced birefringence associated with the differences in thermal expansion between the two materials. A minimal amount of low stress optical adhesive (Dymax OP-66-LS) was used to secure the prisms. The prism stages allow for the external control of the prisms relative rotational orientation. Each prism stage is mounted atop a linear translation stage with the stages oriented orthogonal to each other, where the back prism translation is orthogonal to the optical axis of the cavity.

It was found that the external mounting of the prism stages limited the spectrometer to cavity enhanced absorption measurements at atmospheric pressure. This was required because

spectrum were measured after purging the chamber at atmospheric pressure with dry nitrogen gas. One exception was the prism cavity loss modeling measurements because all measurements were made at a single pressure. Using the external prisms stages, the alignment of the cavity was optimized after evacuating the chamber. Recently, we have mounted the prisms and smaller prism stages (New Focus 9411) inside of a larger vacuum chamber, which is pumped by a 1600 l/s turbomolecular pump.

In this experiment, the prism cavity was aligned and optimized using the pump laser wavelength. A typically empty cavity ringdown time at 1.064 μm was 33-34 μs , which corresponds to a mean photon intracavity pathlength of ~ 10 km. Optimization of the cavity at other wavelengths proved too difficult because of the limited spectral power density generated by the supercontinuum. However, due to the flat dispersion profile of fused silica in the supercontinuum spectral range combined with the fact that the loss is approximately quadratic in the error in Brewster's angle, the Fresnel losses are relatively small. Figure 4 shows the calculated Fresnel loss per prism across the wavelength range of the supercontinuum for a prism aligned at Brewster's angle for 1.064 μm .

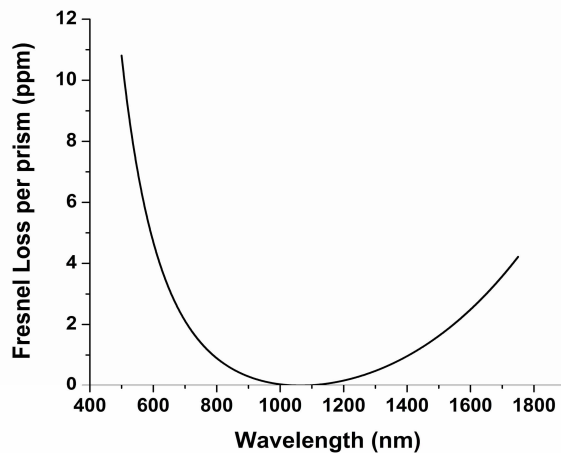


Fig. 4. The calculated Fresnel loss per prism across the visible and near-IR for a fixed prism alignment at Brewster's angle for 1064 nm.

2.2 Supercontinuum generation

The supercontinuum excitation source is generated by pumping ~ 20 meters of a highly nonlinear photonic crystal fiber (SC-5.0-1040, Crystal Fibre) with 1.064 μm light from a diode pumped, Q-switched laser producing 10 ns pulse at a repetition rate of 30 kHz. The pump laser is coupled into the fiber's 5 μm core (N.A. = 0.20) using a 20x microscope objective. The input pulse energy is limited to 34 μJ , or a time averaged power of 1 W, by the optical damage to the input face of the fiber. Figure 5 shows an example of the supercontinuum spectrum later generated after the fiber had been inadvertently broken, reducing the overall fiber length to 13.5 meters. The spectrum was recorded with an optical spectrum analyzer (ANDO AQ-3315E) and shows the supercontinuum spanning from 500 nm to greater than 1750 nm, which extends beyond the near-IR limit of the spectrum analyzer. This source has a spectral brightness of $\sim 40 \text{ kW cm}^{-2} \text{ sr}^{-1} \text{ nm}^{-1}$, approximately 3 orders of magnitude higher spectral brightness than the spatially incoherent light sources that have been used for CEAS studies [15]. Exiting the fiber, the generated supercontinuum is collimated with a 1 cm focal length off axis parabolic mirror and apertured to pass only the central Airy disk of the light emitted by the fiber. The collimated output beam of the fiber, with a beam radius of 3.5 mm, is mode matched to the astigmatic TEM_{00} mode of the cavity using two

broadband spherical mirrors. Using the ABCD formalism, the positions and incident angles of the two spherical mirrors were calculated for 1.064 μm .

A time average power of 180 mW was measured for the generated supercontinuum prior to the cavity input polarizer. As a consequence of the weakly birefringence photonic crystal fiber, the polarization state of the generated supercontinuum is randomly polarized which reduces the total power by 1/2 after the cavity input polarizer. A birefringent supercontinuum fiber has been demonstrated recently [19] and would eliminate much of the current polarization loss.

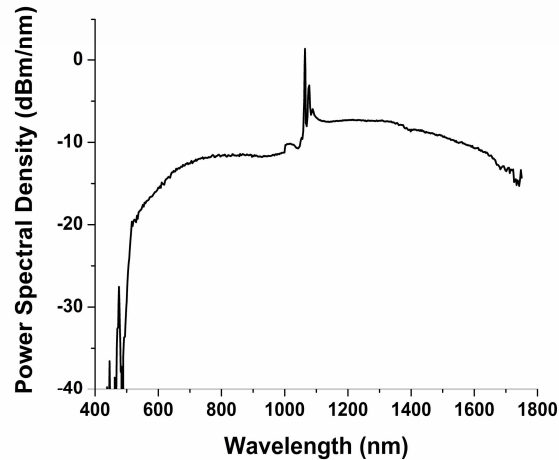


Fig. 5. Spectrum of the supercontinuum generated by pumping 13.5 m of the SC-5.0-1040 fiber with 10 ns, 34 μJ pulses from a Q-switched Nd:YAG laser. The spectrum was observed using an optical spectrum analyzer. The molecular spectra reported elsewhere in this paper were recorded using 20 m of fiber, however the fiber broke before we were able to record the supercontinuum spectrum.

2.3 Cavity enhanced absorption detection

The light transmission of the prism cavity is dispersed using a Czerny-Turner spectrograph (Jobin-Yvon THR1000) with a focal length of 1 m using a 14 cm long by 12 cm high 2400 grove/mm grating allowing wavelengths of <790 nm to be detected. The CCD camera (Andor DU440), cooled to -45 $^{\circ}\text{C}$, images the spectrally dispersed cavity transmission and provides 2048 individual detection channels (13.5 μm x 13.5 μm) with a spectral dispersion of 0.05 $\text{cm}^{-1}/\text{pixel}$ (at $\lambda = 690$ nm). A flip mirror allows the selection of either CCD detection or directs the light to a PMT mounted behind an adjustable slit on the spectrograph. The PMT, a near-IR sensitive Hamamatsu R928, measures the empty cavity ring-down time vs. wavelength. The PMT is thermoelectrically cooled to minimize dark counts and is utilized in a reverse time-correlate single photon counting configuration. In this method a Time to Amplitude Converter (TAC) receives a start pulse from the PMT and a stop pulse from the laser Nd:YAG Q-switch sync out. Converting pulse heights to time delay (with 48.8 ns resolution) gives a histogram of photon flux transmitted by the cavity as a function of time delay from the input laser pulse. The broad bandwidth output of the cavity is filtered to a narrow wavelength interval, typically 1 nm determined by the width of the slit in front of the PMT. The counts versus time delay distribution at each wavelength were fit to a model of an exponential decay with an offset (to account for dark counts in the PMT and stray light). Shot noise weighting was used in the nonlinear, least squares fit. Each fit gave the empty cavity power decay rate, $k(\nu)$ (inverse of the cavity decay time), from which $1-R(\nu)$ is calculated as $k(\nu) t_r$, where t_r is the calculated round trip time in the cavity. To prevent significant "pile-up error" the photon count rate was maintained at or below 700 Hz (i.e. less than 0.024 detected photons per laser pulse) [20]. Typically, each wavelength decay data set included 120,000

detected photons and determined the ring-down time with a fractional uncertainty of 0.04. The first 37 time bins (1.8 μ s) were discarded to avoid any influence from unwanted s-polarized light initially injected into the cavity. S-polarized light decays with a loss of about 50% per round trip. More recently, we obtained a multichannel scaler (Stanford Instruments model SR430) for measuring the decay time. The multichannel scaler is triggered by the Q-switch sync pulse and measures the number of photon counts in each time window. Since the multichannel scaler can count multiple photons per decay, this leads to negligible pile up error and thus removes the count rate limitation.

3. Cavity optical losses

In an effort to characterize and model the various intrinsic optical losses of the prism cavity, the cavity round trip loss was measured in 10 nm increments from 530-770 nm. As Eq. (1) makes clear, the sensitivity of CEAS detection scales inversely with the cavity decay time, *i.e.* the lower the loss and thus longer the decay time, the larger the change in the ratio of the two spectra. Further, one needs to know the empty cavity decay time in order to convert the observed ratio of sample and background transmission spectra into absolute sample absorption versus frequency. In this experiment the vacuum chamber was evacuated to a pressure of ~ 2 mtorr and the prism cavity was aligned and optimized using the pump laser wavelength. The model used considered two loss mechanisms, material scattering, including Rayleigh and surface scattering, and Fresnel loss. Equation (3) shows the model used to fit the experimental data,

$$L(\lambda) = 4 \left(\frac{2\pi\sigma}{\lambda} \frac{n(\lambda)^2 - 1}{\sqrt{n(\lambda)^2 + 1}} \right)^2 + \left(\frac{16\pi n(\lambda) \cos(\theta) \sigma}{\lambda} \right)^2 + \frac{A}{\lambda^4} + \frac{(n(\lambda)^4 - 1)^2}{2n(\lambda)^6} (\delta\theta_1(\lambda)^2 + \delta\theta_2(\lambda)^2) \quad (3)$$

where $n(\lambda)$ is the index of refraction, σ is the prism rms surface roughness, θ is the incident angle inside the prism, A is the Rayleigh scattering prefactor for fused silica and $\delta\theta_1(\lambda)$ and $\delta\theta_2(\lambda)$ are the external angle deviations associated with the frequency dependent Brewster's angle. A nonlinear least squares fit of the data was performed fitting the prism input angle (θ_1), the back prism angle (θ_2), and A with $\sigma = 0.1$ nm and $\theta = 45^\circ$.

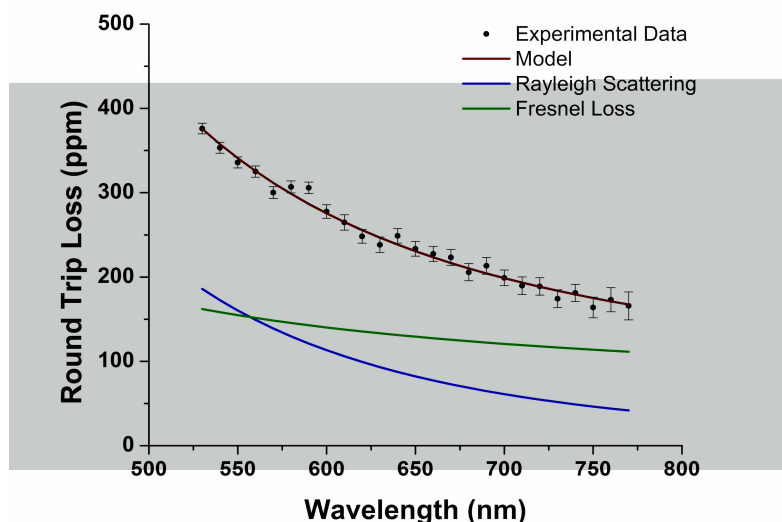


Fig. 6. Fit of the observed round trip cavity loss with Eq. 3, as determined from the ring-down time, as a function of wavelength. The 2σ error bars from the ring-down fits are indicated. Also shown are the individual loss contributions from the dominant loss mechanisms: Rayleigh scattering and Fresnel loss. The resulting fit parameters are given in the text.

Figure 6 shows the least squares fit of the model to experiment, including the individual contributions of the dominant loss mechanisms, Rayleigh scattering in the fused silica and Fresnel loss, to the overall round trip loss of the cavity. The rms error of the fit was 7.28 ppm. From the fit, a Rayleigh scattering coefficient for fused silica of 1.362 ppm/cm at 1064 nm was calculated, which is in good agreement with previous measurements [21]. From the fit $\theta_1 = 54.84^\circ$ and $\theta_2 = 55.03^\circ$ (compared to 55.40° for Brewster's angle at 1.06 μm) were also determined.

4. Broadband detection

A proof of principle test of the spectrometer was performed using the weak b-X ($1\leftarrow 0$) transition of molecular oxygen [1] in the region of 14529 cm^{-1} and the fifth overtone of the acetylene C-H stretch near 18430 cm^{-1} [22]. The empty cavity ringdown time was measured over the absorption region in 2 nm increments and a linear fit was applied to the set of measurements to model the frequency dependent loss of the empty cavity. Note that any overall shift in cavity loss or supercontinuum intensity will result in a baseline shift and will not affect the spectral structure. The fit was then used to calculate the absorption coefficients for each CCD detection channel. Figure 7 shows the recorded cavity transmission spectrum after flushing the cavity at atmospheric pressure with laboratory air along with the predicted spectrum based upon HITRAN [23]. The complete oxygen spectrum was acquired in a series of three measurements (each a separate angle of the spectrograph grating) with a spectral dispersion of 0.05 cm^{-1} (1.5 GHz) /pixel and a CCD integration time of 150 sec per measurement. An average of 110,000 counts/pixel was recorded for each measurement. From the baseline fluctuations, a rms noise equivalent absorption of $5.88 \times 10^{-9}\text{ cm}^{-1}$ or equivalently $7.2 \times 10^{-8}\text{ cm}^{-1}\text{ Hz}^{-1/2}$ was calculated. Signal processing time is negligible and can be done while the CCD integrates further spectra. Note that when one considers that 2048 spectral channels are detected in parallel, this is equivalent to a detection sensitivity of $1.6 \times 10^{-9}\text{ cm}^{-1}\text{ Hz}^{-1/2}$ if a tunable laser is used to scan over the same spectral window. The well-resolved features of the oxygen spectrum have full width half maximum line widths of 0.18 cm^{-1} , compared to the HITRAN predicted pressure broadening width of 0.12 cm^{-1} for the P(7) rotational branch [23].

The spectrum of neat acetylene at atmospheric pressure was recorded at a single grating position with a spectral dispersion of 0.13 cm^{-1} (3.9 GHz)/pixel and an integration time of 30 sec. An average of 40,000 counts/pixel was recorded. As a result of the density of the spectrum and lack of a clear baseline the rms noise equivalent absorption was estimated from two reference spectra acquired with an integration time of 150 sec. A rms noise equivalent absorption of $1.28 \times 10^{-7} \text{ cm}^{-1} \text{ Hz}^{-1/2}$ was calculated. The features of the acetylene spectrum have full width half maximum line widths of 0.44 cm^{-1} , compared with a predicted pressure broadening of 0.26 cm^{-1} from the R(11) rotational branch of the $5\nu_3$ CH stretch [24].

Fig. 8. Cavity enhanced absorption spectrum of the fifth overtone of the acetylene C-H

We have made measurements of the spectrometer baseline noise versus integration time. With fixed experimental conditions, we read the CCD camera once every 10 sec for a total of ~8 hours. Successive CCD readings were averaged for time intervals Δt , with the next Δt time interval integrated as reference spectrum. The ratio of each such pair of spectra was computed and the variance of the ratio computed and averaged across different spectra. This was done for each possible Δt , producing an "Allan variance" type plot of instrument noise versus integration time. It was found that the mean variance (which is proportional to the square of the absorption baseline noise in a computed spectrum) decreased approximately linearly in one over the integration time, as one would predict for uncorrelated noise such as shot noise, up to a time interval of ~90 min, at which point the noise had a minimum, demonstrating the high stability of the supercontinuum source. This time interval represents the maximum time that one should allow between observation of sample and background reference spectra. Note that any change in the spectrum of the generated supercontinuum in the sampled spectral region (expect an overall change in intensity) will generate noise in the calculated spectrum. Also note that one could take some of supercontinuum prior to the cavity and focus it on the input slit of the spectrograph, vertically displaced from the cavity output, producing a second row of intensity on the CCD output. This would provide a reference for any changes in the supercontinuum spectrum while the spectra are being recorded.

5. Conclusion

This proof of principle experiment demonstrates the broadband capabilities of the prism based cavity enhanced spectrometer. Although demonstrated only using the visible portion of the supercontinuum, trace detection across the entire supercontinuum source is possible and an improvement in the detection limits in the NIR is expected as a direct result of the λ^{-4} scattering loss dependence. A prism cavity round trip loss of 34 ppm has been measured at 1570 nm [25]. Ongoing experiments are focused on extending detection into the NIR and moving the prism mounts inside of the vacuum chamber to allow for measurements at partial pressure. In addition, work to improve the duty cycle of the spectrometer by incorporating a higher powered supercontinuum source with anticipated powers of 4-6 W [26] and a truly broadband detection scheme, such as using an FTIR [27, 28] or echelle spectrograph are underway. The high power supercontinuum source should also allow for the optimization of the prism cavity for a given spectral region of interest.

Acknowledgments

The authors are grateful to Pam Chu at NIST for the loan of the optical spectrum analyzer to characterize the supercontinuum spectrum and Tiger Optics LLC for equipment support. This research was supported by the University of Virginia.